Journal of Alloys and Compounds 509 (2011) 8455–8459

Contents lists available at ScienceDirect

Journal of Alloys and Compounds

journal homepage: www.elsevier.com/locate/jallcom

Mechanical and thermal properties of $Tb_2(MoO_4)_3$ crystals

Min Xu [a], Wenlan Gao [a], Huaijin Zhang [a], Xiufeng Cheng [a], Xinguang Xu [a,*], Jiyang Wang [a,*], Robert I. Boughton [b]

[a] State Key Laboratory of Crystal Materials and Institute of Crystal Materials, Shandong University, Jinan 250100, PR China
[b] Department of Physics and Astronomy, Bowling Green State University, Bowling Green, OH 43403, USA

ARTICLE INFO

Article history:
Received 17 June 2010
Received in revised form 17 May 2011
Accepted 3 June 2011
Available online 12 June 2011

Keywords:
Terbium molybdate crystals
Anisotropy
Mechanical and thermal analysis

ABSTRACT

The mechanical and thermal properties of single crystal $Tb_2(MoO_4)_3$ have been systematically studied. The result of microhardness measurement indicates that the crystal belongs to the soft materials category. The thermodynamic parameters obtained from DTA analysis were used for determining the type of liquid–solid interface during crystal growth. Negative thermal expansion along the *c*-axis was observed, and this behavior was attributed to the bent Tb–O–Mo bonds. The specific heat of the crystal was measured to be 0.122 cal g^{-1} K^{-1} at 293.15 K. The thermal conductivity of $Tb_2(MoO_4)_3$ at room temperature was found to be smaller than that of representative ferroelectric $LiNbO_3$.

1. Introduction

Several rare-earth tungstates and molybdates were discovered to possess unusual fluorescence, laser, piezoelectric, ferroelectric and ferroelastic properties. Most of these materials crystallize in the $Ln_2(MO_4)_3$ structure with orthorhombic space group *Pba2* at room temperature, where Ln is a rare-earth element (Gd, Eu, Tb, Dy, Ho, etc.) and M is a tungstate or molybdate element [1]. These materials undergo a ferroelectric–paraelectric phase transition over the temperature range of about 150–190 °C with the addition of various rare-earth elements Ln [2]. In contrast to some representative ferroelectrics (e.g., $LiNbO_3$, $BaTiO_3$), the ferroelectricity of these materials is due to an elastic instability, so they are classified as improper ferroelectrics. In the $Ln_2(MO_4)_3$ family, gadolinium molybdate [$Gd_2(MoO_4)_3$] is the most interesting crystal due to some excellent properties that it exhibits [3–9]. For instance, the coercive field of the crystal is about 2.5(~5) kV cm^{-1} [9] which is lower than that of $LiNbO_3$ (40 kV cm^{-1}) [10]. Thus, the ferroelectric domains in $Gd_2(MoO_4)_3$ can be reversed more easily than $LiNbO_3$ under an applied electric field. The nonlinear optical coefficients are $d_{31} = -2.49$ pm V^{-1} and $d_{32} = 2.42$ pm V^{-1} for $Gd_2(MoO_4)_3$ [9], which are all close to those of $LiNbO_3$ ($d_{31} = -4.35$ pm V^{-1}, $d_{22} = 2.10$ pm V^{-1}) [11].

As an isomorph of $Gd_2(MoO_4)_3$, terbium molybdate [$Tb_2(MoO_4)_3$] is ferroelectric and ferroelastic with orthorhombic space group *Pba2* at room temperature [12]. However, it crystallizes in a tetragonal structure with space group $P\bar{4}2_1m$ when the temperature is raised above its ferroelectric–paraelectric and ferroelastic–paraelastic transition temperature (163 ± 1 °C), and the number of formula units per unit cell decreases to 2 [12,13]. It is assumed that $Tb_2(MoO_4)_3$ is also a potential multipurpose material because most properties of the crystal are similar to $Gd_2(MoO_4)_3$ [9,12]. Though some previous researchers have reported on some properties of $Tb_2(MoO_4)_3$, most of them have been applied to study only the phase transition [12,14,15]. We have focused on $Tb_2(MoO_4)_3$ to study the coupling among its magnetic, electric and optical properties [16]. For such interactive coupling, the mechanical and thermal properties greatly influence the range of application of the material. For instance, the hardness of a crystal can be regarded as a major indicator of what the mechanical properties are like, and as an indicator of whether the material can be processed easily. The limit on the applied external field power is determined by the thermal conductivity of a crystal in optical configuration especially the nonlinear optical or laser system.

In this paper, we present measurements of the mechanical and thermal properties of single crystal $Tb_2(MoO_4)_3$, including microhardness, DTA, thermal expansion, specific heat, thermal diffusivity and thermal conductivity. The influence of these properties on $Tb_2(MoO_4)_3$ is also discussed in detail.

2. Experimental

High quality $Tb_2(MoO_4)_3$ crystals were pulled from the melt using the Czochralski method [17,18]. The crystals are transparent and crack-free with approximate dimensions of Φ 25 mm × 20 mm, weighing about 30–50 g. The experimental samples for various measurements were cut from the as-grown crystals. As a preliminary, the density and microhardness of the samples were measured.

* Corresponding author. Fax: +86 531 88364848.
E-mail addresses: xgxu@sdu.edu.cn (X. Xu), jywang@sdu.edu.cn (J. Wang).

0925-8388/$ – see front matter © 2011 Elsevier B.V. All rights reserved.
doi:10.1016/j.jallcom.2011.06.001

Table 1
Experimental density of $Tb_2(MoO_4)_3$ at room temperature (301.2 K, $\rho_{water} = 0.9963\ g\,cm^{-3}$).

	Sample 1	Sample 2	Sample 3
m (g)	4.865	1.511	2.652
m' (g)	3.814	1.185	2.078
ρ_{exp} ($g\,cm^{-3}$)	4.612	4.618	4.603
ρ_{ave} ($g\,cm^{-3}$)	4.611		

2.1. Density and microhardness

The theoretical density of $Tb_2(MoO_4)_3$ was calculated using the ratio of the cell mass to cell volume. While, the experimental density was measured by the buoyancy method at room temperature (301.2 K), and is obtained using the following equation:

$$\rho_{exp} = \frac{m\rho_{water}}{m - m'} \quad (1)$$

where m is the mass of crystal sample in air, m' is the mass when the sample immersed in distilled water, and ρ_{water} is the density of water at the measurement temperature.

The microhardness normal to the (1 0 0), (0 1 0) and (0 0 1) faces of $Tb_2(MoO_4)_3$ in wafer form was measured with a digital microscopic Weiss sclerometer (HXS-1000A) at room temperature. The tested samples were carefully polished. During the measurement, two different loads (5 g, 10 g) were applied, both of which were maintained for 1 s.

2.2. Differential thermal analysis (DTA)

The differential thermal analysis (DTA) method was used to determine the melting point and enthalpy of fusion for the $Tb_2(MoO_4)_3$ crystal. The measurement was made with a Diamond model TG/DTA made by Perkin-Elmer. Powder samples with weight up to 11.552 mg were used in the measurement. The sample was kept in an Al_2O_3 crucible and another empty Al_2O_3 crucible was used as reference as they are heated together at a constant rate (10 K/min). The heat flow curve was recorded from 573 to 1468 K.

2.3. Thermal expansion

The thermal expansion of the $Tb_2(MoO_4)_3$ crystal was measured over the temperature range from 301.15 to 769.15 K using a thermal dilatometer (Perkin-Elmer Co.). A rectangular piece of the crystal with dimensions of 4 mm × 5 mm × 6 mm ($a \times b \times c$) was used. During the measurement, the sample was heated at a constant rate of 5 K/min and the thermal expansion ratio ($\Delta L/L_0$) vs. temperature curves along the crystallographic a-, b- and c-axes were obtained.

2.4. Specific heat

The specific heat was measured using a differential scanning calorimeter (Diamond DSC) under N_2 flow at constant pressure. A small sample weighing 40.01 mg was used. The temperature was raised from 293.15 to 573.15 K at a constant rate of 5 K/min. The results were obtained using the software supplied with the apparatus (Perkin-Elmer Co.).

2.5. Thermal diffusivity

The thermal diffusivity of $Tb_2(MoO_4)_3$ was measured by the laser flash method on a Netzsch Nanoflash model LFA 447 apparatus over the temperature range from 303.15 to 543.15 K. Three square (6 mm × 6 mm × 2 mm) wafers cut from the crystal with polished faces perpendicular to the crystallographic a-, b- and c-axes and coated with graphite on both sides were used to carry out the measurements. During the experiment, a short light pulse heats the front surface of the plane-parallel crystal wafer and the temperature rise on the rear surface is measured versus time using an IR-detector. The thermal diffusivity of the crystal was calculated using analytical software provided with the apparatus.

3. Results and discussion

3.1. Density and microhardness

The theoretical density of $Tb_2(MoO_4)_3$ is calculated to be $4.628\ g\,cm^{-3}$ based on the lattice information given in Ref. [19]. By comparison, the buoyancy method measurements give a corresponding average experimental density of $4.611\ g\,cm^{-3}$ (Table 1) in good agreement with the theoretical value.

Table 2
Microhardness of $Tb_2(MoO_4)_3$.

Load (g)	Vickers microhardness ($kg\,mm^{-2}$)		
	(1 0 0) Wafer	(0 1 0) Wafer	(0 0 1) Wafer
5[a]	255	272	256
10[a]	271	263	310
15–200[b]			630 ± 30

[a] This work for $Tb_2(MoO_4)_3$.
[b] Microhardness of $LiNbO_3$ (Ref. [20]).

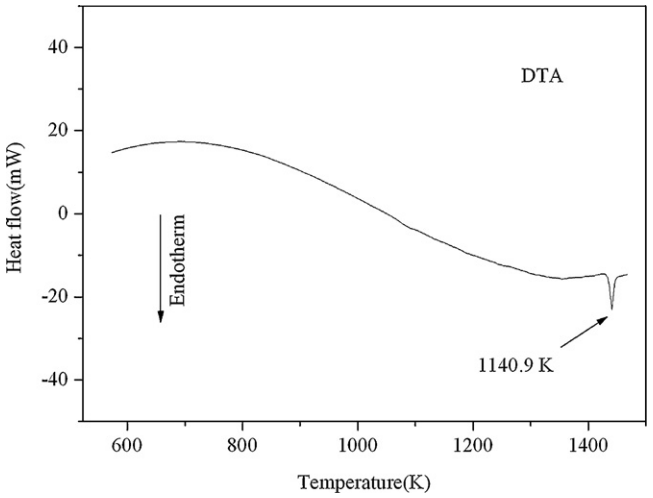

Fig. 1. DTA curve of $Tb_2(MoO_4)_3$.

The microhardness values of the (1 0 0), (0 1 0) and (0 0 1) surfaces of $Tb_2(MoO_4)_3$ wafers are listed in Table 2. For comparison, the microhardness of $LiNbO_3$ is also presented [20]. From the table, one can see that the Vickers microhardness values are not as large for $Tb_2(MoO_4)_3$, which means that the crystal belongs to the soft materials category and can be easily processed.

3.2. DTA analysis

Since the melting point (T_E), the molar enthalpy of fusion ($\Delta_{fus}H_m$) and the molar entropy of fusion ($\Delta_{fus}S_m$) are important thermodynamic parameters in determining actual and simulated crystal growth rates, DTA analysis were carried out over a wider temperature range than what was reported in a previous paper [16] where the phase transition was determined. Fig. 1 shows the DTA curve of $Tb_2(MoO_4)_3$, in which there is only one endothermic peak in the measurement temperature range. This peak exhibits the characteristics of a melting process, and the peak temperature of 1440.9 K is identified as the melting point of $Tb_2(MoO_4)_3$, a value which is slightly higher than that reported by Nassau [1]. The molar enthalpy of fusion $\Delta_{fus}H_m$ is derived from the DTA curve using the area integration method included in the DTA analytical software provided by the manufacturer. The molar entropy of fusion, $\Delta_{fus}S_m$, can be calculated using the thermodynamic equation shown as $\Delta_{fus}S_m = \Delta_{fus}H_m/T_E$. The three thermodynamic parameters are listed in Table 3.

Table 3
Thermodynamic parameters of $Tb_2(MoO_4)_3$ obtained from DTA measurements.

Thermodynamic parameter	Value
T_E (K)	1440.9
$\Delta_{fus}H_m$ ($J\,mol^{-1}$)	13186.2
$\Delta_{fus}S_m$ ($J\,mol^{-1}\,K^{-1}$)	9.15

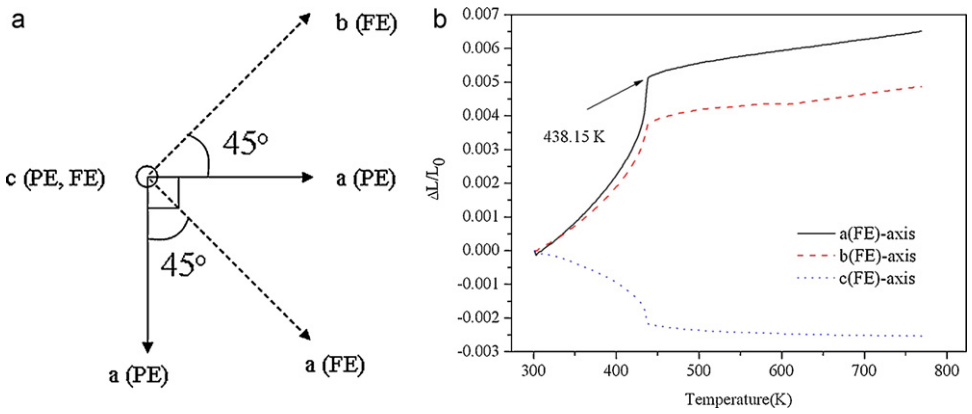

Fig. 2. (a) Orientation of coordinate system for crystallographic axes in tetragonal phase (PE) and orthorhombic phase (FE). (b) Thermal expansion ratio curves of $Tb_2(MoO_4)_3$.

In addition, the Jackson factor [21], which is usually used to predict the roughness of the crystal growth interface can be calculated as follows:

$$\alpha = \frac{L}{\kappa T_E} f = \frac{\Delta_{fus} H_m}{RT_E} f = \frac{\Delta_{fus} S_m}{R} f \quad (2)$$

where α is the Jackson factor, L is the latent heat of crystallization, k is the Boltzmann constant, R is the gas constant, T_E is the melting point, and f is the fraction of the binding energy associated with the layer, which depends on the crystal face and is always less than unity. If $\alpha \leqq 2$, the interface is considered a rough surface; otherwise, it is considered a smooth surface. The calculated Jackson factor value for $Tb_2(MoO_4)_3$ is $\alpha = 1.10f$. Since it is less than 2, the liquid–solid interface most probably is a rough surface when a $Tb_2(MoO_4)_3$ crystal is pulled from the melt, according the Jackson theory. As a result the growth rate can be kept relatively high (in Ref. [12], a pulling rate of 1 cm/h was utilized).

3.3. Thermal expansion

The thermal expansion coefficient $[\alpha_{ij}]$ of a crystal is a symmetric second rank tensor [22]. In the principal coordinate system the $[\alpha_{ij}]$ tensor is diagonal,

$$\begin{pmatrix} \alpha_{11} & 0 & 0 \\ 0 & \alpha_{22} & 0 \\ 0 & 0 & \alpha_{33} \end{pmatrix} \quad \text{or} \quad \begin{pmatrix} \alpha_1 & 0 & 0 \\ 0 & \alpha_2 & 0 \\ 0 & 0 & \alpha_3 \end{pmatrix}$$

The quantities α_1, α_2, and α_3 are the principal components of the thermal expansion coefficient tensor. $Tb_2(MoO_4)_3$ is orthorhombic in the ferroelectric–ferroelastic phase (abbreviated FE) and tetragonal in the paraelectric–paraelastic phase (abbreviated PE), so, there are three independent principal components (α_1, α_2, α_3) of the thermal expansion coefficient tensor below the phase transition temperature and only two independent principal components ($\alpha_1 = \alpha_2$, α_3) above the phase transition temperature. According to previous structure analysis [13,23], the tetragonal unit cell in the PE phase possesses half the volume of the FE phase unit cell with $a_{PE} \approx a_{FE}/\sqrt{2}$, and is rotated by 45° in the FE a–b plane. While $c_{PE} \approx c_{FE}$ and they are parallel to each other, the orientation of the coordinate system for the crystallographic axes in the PE and FE phases is shown in Fig. 2(a). When the thermal expansion is recorded along the orthorhombic crystallographic a-, b- and c-axis, the three corresponding principal components $\alpha_1(=\alpha_a)$, $\alpha_2(=\alpha_b)$, $\alpha_3(=\alpha_c)$ can be obtained in the FE phase temperature range, while the corresponding components are recorded as $\alpha_{[1\,1\,0]}$, $\alpha_{[-1\,1\,0]}$ and $\alpha_{[0\,0\,1]}$ in the PE phase temperature range (see Fig. 2(a)). However, the quadratic representation of a symmetric second rank tensor is either an ellipsoid or hyperboloid of revolution about the four-fold axis (c-axis) for a tetragonal crystal [22]. So the components $\alpha_{[1\,1\,0]}$ and $\alpha_{[-1\,1\,0]}$ of tetragonal $Tb_2(MoO_4)_3$ over the PE phase temperature range can be considered to be equal. The average experimental values for $\alpha_{[1\,1\,0]}$ and $\alpha_{[-1\,1\,0]}$ is used as the principal component α_1 of the tetragonal $Tb_2(MoO_4)_3$ crystal, while $\alpha_{[0\,0\,1]}$ is another principal component (α_3) because there is no change in the orientation of c-axis with increasing temperature.

Fig. 2(b) shows the thermal expansion ratio ($\Delta L/L_0$) curves of $Tb_2(MoO_4)_3$, where ΔL is the length change of the sample when the temperature is raised, and L_0 is the sample length at the initial temperature T_0 (301.15 K). From Fig. 2(b), one can see that an inflection occurs at about 438.15 K on each curve. This change can be attributed to the intrinsic ferroelectric–paraelectric and ferroelastic–paraelastic phase transitions. Interestingly, negative thermal expansion behavior along the c-axis has been observed, which is similar to the result presented in Ref. [24]. This behavior can be explained by focusing on the polyhedron fragment of the $Tb_2(MoO_4)_3$ structure [25] that is formed by TbO_7 polyhedra and MoO_4 tetrahedra linked together at their common corners. The Tb–O–Mo bonds along the c-axis become weak when the temperature is raised. They arise from rotational coupling and bend under the influence of the other polyhedra. Nevertheless, the rigid TbO_7 polyhedra and MoO_4 tetrahedra do not significantly change because of the stronger Tb–O and Mo–O linkages. The ionic distance between Tb^{3+} and Mo^{6+} is subsequently shortened. Finally, the thermal expansion along the c-axis becomes negative at the macroscopic level.

The average linear thermal expansion coefficient can be calculated according to the following equation:

$$\overline{\alpha}(T_0 \rightarrow T) = \frac{\Delta L/L_0}{\Delta T} \quad (3)$$

where $\overline{\alpha}(T_0 \rightarrow T)$ is the average linear thermal expansion coefficient over the measured temperature range, $\Delta T = T - T_0$ is the temperature change, and $\Delta L/L_0$ is the thermal expansion ratio. Considering that the principal expansion components will be changed because of the phase transition, the thermal expansion coefficient is calculated over separate temperature ranges. The calculated principal thermal expansion coefficient components over these temperature ranges are listed in Table 4 (the magnitudes of these results are in good agreement with those reported by Abrahams et al. [24]. For example, the linear thermal expansion coefficient of a-axis may be estimated to be $3.4 \times 10^{-5}\ K^{-1}$ over the temperature range of 296–436 K according to the three order expression given by them). From the table, it can be seen that the crystal possesses a large anisotropic thermal expansion, so crystalline $Tb_2(MoO_4)_3$ should be cooled to room temperature at a slow rate after growth in order to avoid cracking.

Table 4
The principal thermal expansion coefficient components of $Tb_2(MoO_4)_3$.

Principal thermal expansion coefficient (10^{-5} K^{-1})	Orthorhombic phase (301.15–438.15 K)	Tetragonal phase (438.15–769.15 K)
α_1	3.74	0.376
α_2	2.74	
α_3	−1.58	−0.112

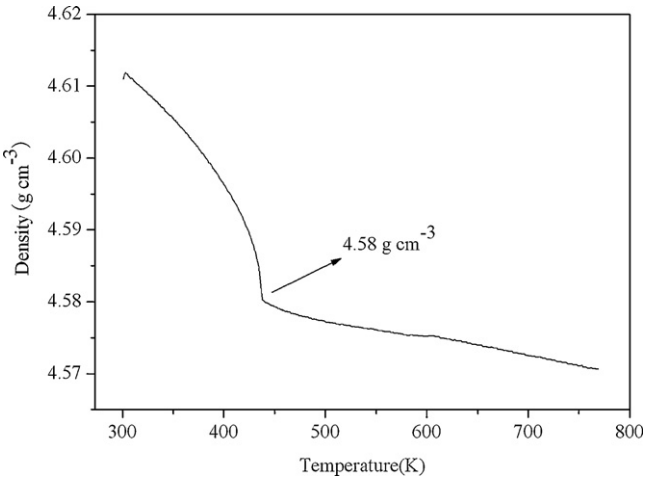

Fig. 3. Density as a function of temperature for $Tb_2(MoO_4)_3$.

Additionally, the volume of the rectangular crystal sample changes when thermal expansion takes place, and the density varies accordingly. The density of $Tb_2(MoO_4)_3$ at temperature T can be calculated based on the thermal expansion ratio presented in Fig. 2(b). The density as a function of temperature for $Tb_2(MoO_4)_3$ is shown in Fig. 3. From the figure, one can see that the density decreases to 4.58 g cm^{-3} at 438.15 K when the phase transition takes place. This value agrees well with the calculated density of tetragonal $Tb_2(MoO_4)_3$ using the crystallographic data [13], which gives a value of 4.59 g cm^{-3}.

3.4. Specific heat

Fig. 4 shows the measured specific heat curve vs. temperature for $Tb_2(MoO_4)_3$. In the figure, a sharp peak appears at 433.15 K. It is attributed to the phase transition of $Tb_2(MoO_4)_3$. The small difference in the transition temperature observed in the specific heat and in the thermal expansion measurements is probably caused by experimental error. The specific heat value at 293.15 K is 0.509 J g^{-1} K^{-1} (406.01 J mol^{-1} K^{-1}), also equal to 0.122 cal g^{-1} K^{-1}, a value that is slightly greater than that of $Gd_2(MoO_4)_3$ (~0.1 cal g^{-1} K^{-1}) [9]. In general, the larger specific heat that a crystal possesses, the smaller the resulting change in temperature when it gains or loses a given amount of heat. Since $Gd_2(MoO_4)_3$ is typically applied in nonlinear optical configurations [9], one can deduce that similar potential applications are also possible for $Tb_2(MoO_4)_3$ because of its larger specific heat.

The dependence of the specific heat capacity on temperature can be expressed as follows:

$$C_p = A + BT + CT^{-2} \quad (4)$$

where A, B and C are empirical fitting constants, C_p is the specific heat at constant pressure with units of J mol^{-1} K^{-1} and T is the absolute temperature. Based on the measured values of C_p, the dependence of C_p on T is fitted as:

$$C_p = -1.54049 \times 10^2 + 1.77213T + 3.585574 \times 10^6 T^{-2}$$

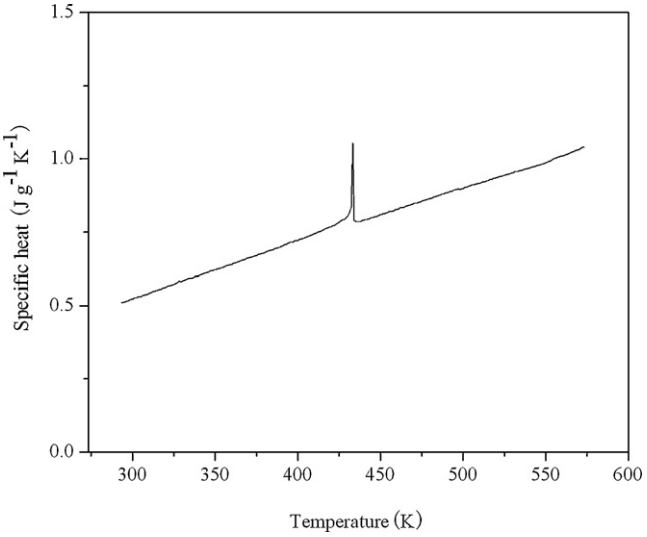

Fig. 4. Specific heat vs. temperature curve of $Tb_2(MoO_4)_3$.

over the temperature range of 293.15–423.15 K with a residual $R^2 = 0.99961$, and as:

$$C_p = -0.73287 \times 10^2 + 1.53601T + 5.63874 \times 10^6 T^{-2}$$

over the temperature range of 438.15–573.15 K with a residual $R^2 = 0.99895$.

3.5. Thermal diffusivity and thermal conductivity

The thermal diffusivity and thermal conductivity of a crystal are related to each other using the following equation:

$$k = \lambda \rho C_p \quad (5)$$

where k, λ, ρ and C_p denote the thermal conductivity, thermal diffusivity, density and specific heat of the crystal, respectively. The thermal conductivity and thermal diffusivity of a crystal are also symmetric second-rank tensors [22], so they can be written in exactly the same way as $[k_{ij}]$ and $[\lambda_{ij}]$. Both the $[k_{ij}]$ and $[\lambda_{ij}]$ tensors are diagonal in the principal coordinate system. There are three independent principal components for orthorhombic $Tb_2(MoO_4)_3$, but only two for tetragonal $Tb_2(MoO_4)_3$. Similar to the analysis of the thermal expansion coefficient tensor, the thermal diffusivity along the crystallographic c-axis remains as the principal component λ_3 for both the orthorhombic and tetragonal phases. The thermal diffusivity along the crystallographic a- and b-axes represents the other two principal components λ_1 and λ_2 in the orthorhombic coordinate system, but they are designated as $\lambda_{[1\,1\,0]}$ and $\lambda_{[-1\,1\,0]}$ in the tetragonal coordinate system (Fig. 2(a)) when the temperature is above the phase transition point. Accordingly, $\lambda_{[1\,1\,0]}$ and $\lambda_{[-1\,1\,0]}$ are assumed to be equal to each other, and their average can be used as the principal component λ_1 for tetragonal $Tb_2(MoO_4)_3$. Finally, the principal thermal conductivities (k_1, k_2, k_3) of $Tb_2(MoO_4)_3$ can be calculated using Eq. (5).

Fig. 5 shows the principal thermal diffusivity components of $Tb_2(MoO_4)_3$ over the temperature range from 303.15 to 543.15 K with about a 30 K interval between measured temperature points. To our knowledge, this is the first time the measurement of these anisotropic coefficients of $Tb_2(MoO_4)_3$ has been carried out. Similar to the measurements of thermal expansion and specific heat, anomalous behavior is observed near the transition temperature. The three principal thermal diffusivity components of the crystal are $\lambda_1 = 0.604$ mm^2 s^{-1}, $\lambda_2 = 0.631$ mm^2 s^{-1} and $\lambda_3 = 0.644$ mm^2 s^{-1} at 303.15 K.

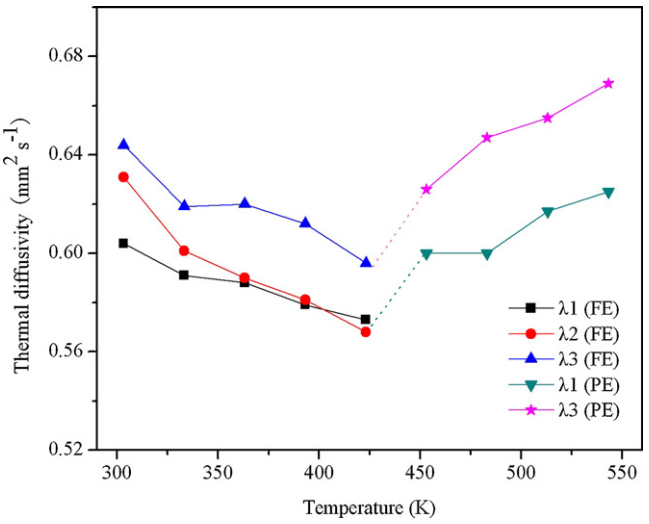

Fig. 5. Principal thermal diffusivity components of $Tb_2(MoO_4)_3$. FE, orthorhombic phase; PE, tetragonal phase.

Table 5
The principal thermal conductivity components of $Tb_2(MoO_4)_3$.

Temp. (K)	303	333	363	393	423	453	483	513	543
k_1	1.474	1.607	1.749	1.887	2.044	2.239	2.393	2.600	2.781
k_2	1.539	1.634	1.755	1.894	2.026				
k_3	1.571	1.683	1.844	1.995	2.126	2.336	2.580	2.764	2.979

Based on the data presented in Figs. 3–5, the calculated principal thermal conductivities of $Tb_2(MoO_4)_3$ at different temperatures are listed in Table 5. As shown in the table, it is observed that $Tb_2(MoO_4)_3$ possesses a small anisotropic thermal conductivity. The value along the *c*-axis (k_3) is relatively the largest. However, the thermal conductivity of the crystal is not very large when compared to other representative ferroelectric crystals, such as $LiNbO_3$ ($k = 5.234\ W\ m^{-1}\ K^{-1}$) [26], so avoidance of thermal shock is important when the crystal is used in any application.

4. Conclusions

A study of the primary mechanical and thermal properties of single crystal $Tb_2(MoO_4)_3$ is reported in this paper. Microhardness measurements show that the crystal possesses a low hardness value and can therefore be easily processed. Determination of the thermodynamic parameters from DTA measurements indicates the liquid–solid interface is most probably a rough surface when the crystal is pulled from melt. The $Tb_2(MoO_4)_3$ crystal exhibits a large anisotropic thermal expansion. The negative expansion behavior along the *c*-axis can be ascribed to the bending of the Tb–O–Mo bonds as the temperature is increased. A peak in the specific heat occurs at about 433.15 K, and indicates the presence of an intrinsic phase transition. Abnormal behavior can also be observed in the dependence of the thermal diffusivity on temperature. Both the anisotropy and specific value of the thermal conductivity for $Tb_2(MoO_4)_3$ are small, and thus indicate that avoidance of thermal shock is important when the crystal is employed in any application.

Acknowledgements

This work is supported by National Natural Science Foundation of China (50590401) and a grant of 973 program (2010CB833103).

References

[1] K. Nassau, J.W. Shiever, E.T. Keve, J. Solid State Chem. 3 (1971) 411.
[2] H.J. Borchardt, P.E. Bierstedt, J. Appl. Phys. 38 (1967) 2057.
[3] M. Kestigian, J. Am. Ceram. Soc.: Discuss. Notes 48 (1965) 544.
[4] L.E. Cross, A. Fouskova, S.E. Cummins, Phys. Rev. Lett. 21 (1968) 812.
[5] H.J. Borchardt, P.E. Bierstedt, Appl. Phys. Lett. 8 (1966) 50.
[6] K. Megumi, H. Yumoto, S. Ashida, et al., Mater. Res. Bull. 9 (1974) 391.
[7] B.S. Red'kin, V.N. Kurlov, et al., J. Cryst. Growth 104 (1990) 77.
[8] A. Yu, Bunkin, J. Cryst. Growth 123 (1992) 459.
[9] A.A. Kaminskii, A.V. Butashin, H.J. Eichler, et al., Opt. Mater. 7 (1997) 59.
[10] K. Nakamura, T. Hatanaka, H. Ito, Jpn. J. Appl. Phys. 40 (4A) (2001) L337–L339.
[11] R.C. Miller, W.A. Nordland, P.M. Bridenbaugh, J. Appl. Phys. 42 (1971) 4145.
[12] E.T. Keve, S.C. Abrahams, K. Nassau, et al., Solid State Commun. 8 (1970) 1517.
[13] B. Dorner, J.D. Axe, G. Shirane, Phys. Rev. B 6 (1972) 1950.
[14] B.A. Strukov, S.A. Taraskin, I.V. Shnaidshtein, A. Onodera, H. Haga, B.S. Red' kin, J. Exp. Theor. Phys. 81 (1995) 202.
[15] B.A. Strukov, A. Onodera, S.A. Taraskin, I.V. Shnaidshtein, B.S. Red'kin, H. Haga, Ferroelectrics 185 (1996) 181.
[16] S. Peng, P. Yang, W. Cai, et al., J. Appl. Phys. 105 (2009) 061622.
[17] M. Xu, Y.G. Yu, H.J. Zhang, J.Y. Wang, J. Rare Earth 27 (2009) 192.
[18] M. Xu, Y.G. Yu, H.J. Zhang, X.Q. Yu, J.Y. Wang, J. Synth. Cryst. (In Chinese) 37 (2008) 1415.
[19] JCPDS diffraction file: 84-0085.
[20] K.G. Subhadra, K. Kishan Rao, D.B. Sirdeshmukh, Bull. Mater. Sci. 23 (2000) 147.
[21] K.A. Jackson, Liquid Metals and Solidification, Cleveland, 1958, p. 174.
[22] J.F. Nye, Physical Properties of Crystals, Oxford, 1985.
[23] J.D. Axe, B. Dorner, G. Shirane, Phys. Rev. Lett. 26 (1971) 519.
[24] S.C. Abrahams, J.L. Bernstein, F. Lissalde, K. Nassau, J. Appl. Cryst. 11 (1978) 699.
[25] C. Svensson, S.C. Abrahams, J.L. Bernstein, J. Chem. Phys. 71 (1979) 5191.
[26] S.H. Yao, J.Y. Wang, et al., J. Alloys Compd. 455 (2008) 501.